Food & Function

ROYAL SOCIETY OF CHEMISTRY

PAPER

View Article Online
View Journal | View Issue

Cite this: *Food Funct.*, 2022, **13**, 11236

The mechanism of ginger and its processed products in the treatment of estradiol valerate coupled with oxytocin-induced dysmenorrhea in mice *via* regulating the TRP ion channel-mediated $ERK_{1/2}$/NF-κB signaling pathway†

Xiaoqin Liu, ‡[a,b] Xianglong Meng,‡[a,b] Xiaojuan Su,[a,b] Kele Ren,[a,b] Chenxu Ning, [a,b] Xiaoming Qi[a,b] and Shuosheng Zhang*[a,b]

Ginger (Rhizoma zingiberis, RZ) has been used as a food, spice, supplement, flavoring agent, and as an edible herbal medicine. It is characterized by its pungency and aroma, and is rich in nutrients with remarkable pharmacological effects. It is used in traditional medicine clinics to treat diseases and symptoms, such as colds, headache, and primary dysmenorrhea (PD). In China, a variety of processed products of RZ are used as herbal medicines, such as baked ginger (BG) or ginger charcoal (GC) to treat different diseases and symptoms. However, the molecular mechanism of the therapeutic effect of RZ and its processed products (RZPPs, including BG or GC) against PD has not been well characterized. Moreover, whether the transient receptor potential (TRP) ion channels are involved in this process is not clear. In the present study, UHPLC-Q-TOF MS was adopted to analyse the differential quality markers (DQMs) between RZ and RZPPs. In addition, differential metabolomics (DMs) was acquired between RZ- and RZPPs-treated estradiol valerate coupled with an oxytocin-induced PD mouse uterus using untargeted metabolomics (UM). A correlation analysis between DQMs and DMs was also conducted. Benzenoids, lipids, and lipid-like molecules were the main DQMs between RZ and RZPPs. RZ and RZPPs were found to improve the pathological status of the uterus of a PD mouse, with significantly decreased serum levels of E_2, $PGF_{2\alpha}$, TXB_2 and remarkably increased levels of PROG and 6-keto-$PGF_{1\alpha}$. Moreover, RZ and RZPPs alleviated PD in mice *via* regulating the TRP ion channel-mediated $ERK_{1/2}$/NF-κB signaling pathway. Our results indicate that the therapeutic effect of RZ and RZPPs against PD may be mediated by regulating the TRP ion channel-mediated $ERK_{1/2}$/NF-κB signaling pathway, and provide a reference for the development of new dietary supplements or medicines.

Received 29th June 2022,
Accepted 11th September 2022

DOI: 10.1039/d2fo01845d

rsc.li/food-function

Introduction

Primary dysmenorrhea (PD) is driven by a non-pelvic organic lesion and its onset typically occurs during puberty with an incidence of up to 90%.[1,2] The main clinical symptom of PD is pain. Onset of PD is closely associated with several factors, including prostaglandin (PG), oxytocin, estrogen, progesterone, endothelin, nitric oxide, calcium (Ca^{2+}), and β-endorphin.[3]

[a]*College of Chinese Materia Medica and Food Engineering, Shanxi University of Chinese Medicine, Jinzhong 030619, Shanxi, China.*
E-mail: zhangshuosheng@aliyun.com
[b]*Shanxi Key Laboratory of Traditional Herbal Medicines Processing, Jinzhong 030619, Shanxi, China*

†Electronic supplementary information (ESI) available: Fig. S1: HPLC chromatogram of 6-gingerol (A), Rhizoma zingiberis (B), baked ginger (C), and ginger charcoal (D). Fig. S2: the DQMs between RZ and RZPPs. (A) Total ion chromatograms in the negative ion mode; (B) volcano plots between RZ and BG in negative ion mode; (C) volcano plots between BG and GC in negative ion mode; (D) PCA score plot for each group in negative ion mode; (E) OPLS-DA score plots between RZ and BG in negative ion mode; (F) 200-time permutations were performed and plotted between RZ and BG in negative ion mode. (G) OPLS-DA score plots between BG and GC in negative ion mode; (H) 200-time permutations were performed and plotted between BG and GC in negative ion mode. Fig. S3: UM results. PCA score plot for each group in positive (A) and negative (H) ion mode. OPLS-DA score plots and 200-time permutations were performed and plotted between different groups in positive (B)–(G) and negative (I)–(N) ion mode. Table S1: the 6-gingerol, 10-gingerol, 6-shogaol, and 8-shogaol contents in RZ and RZPPs. Table S2: DQMs between RZ and BG. Above: DQMs up-regulated; below: DQMs down-regulated. Table S3: DQMs between BG and GC. Above: DQMs up-regulated; below: DQMs down-regulated. Table S4: differential metabolites (DMs) in PD mice treated with RZ and RZPPs. N: normal group; C: control group; RZ: Rhizoma zingiberis group; BG: baked ginger group; GC: ginger charcoal group; above: up-regulated DMs; below: down-regulated DMs. See DOI: https://doi.org/10.1039/d2fo01845d

‡These authors contributed equally to this work.

Specifically, excessive prostaglandin $F_{2\alpha}$ ($PGF_{2\alpha}$) during the menstrual phase can lead to uterine spasmodic contraction resulting in regional ischemia, hypoxia, and reduced blood flow, which are the leading causes of PD.[4] In addition, Ca^{2+} is involved in PD by affecting the synthesis and release of partial neurotransmitters *in vivo*. In modern medicine, non-steroidal anti-inflammatory drugs (NSAID), Ca^{2+} antagonists, and β-receptor agonists are mainly used to alleviate symptoms of PD; however, the therapeutic effect is unsatisfactory, and these drugs cause varying degrees of adverse events.[5] Transient receptor potential (TRP) ion channels were reported to play a role in the treatment of PD. Upon activation, they can either induce cation influx (such as Ca^{2+}) to activate Ca^{2+}-dependent protease and cause damage to the cytoskeleton[6] or indirectly regulate the $PGF_{2\alpha}$ level, leading to alleviation of PD.[7]

TRP ion channels are non-selective cation channels distributed on cell membranes or intracellular organelle membranes. There are 7 subfamilies, that include TRPC, TRPV, TRPM, TRPN, TRPA, TRPP, and TRPML, of which the latter two are evolutionarily more distant.[8] TRPV1 and TRPM8 channel proteins play important roles in the onset and development of PD.[9,10] The TRPV1 channel protein is involved in the pathology of post-inflammatory hyperalgesia in PD after activation by multiple ligand-like substances, inflammatory mediators (such as arachidonic acid metabolites), and tissue injury stimuli.[11,12] The TRPM8 channel protein can be activated by cold temperatures (<28 °C) or in response to pain, to induce a cation influx (including Ca^{2+}), affecting the initiation of PD.[11,13–15] Through this mechanism, activated Ca^{2+}/calmodulin-dependent protein kinase II (CaMK II) can up-regulate the downstream extracellular regulated protein kinases ($ERK_{1/2}$). Phosphorylated $ERK_{1/2}$ can subsequently initiate the expression of nuclear factor-κB (NF-κB), and thereby regulate the expression of cyclooxygenase-2 (COX-2). Studies have shown that COX-2 is an important rate-limiting enzyme involved in $PGF_{2\alpha}$ transformation and synthesis, which supports its potential role in the treatment of PD.[16–18]

Ginger (Rhizoma zingiberis, RZ) originates from *Zingiber officinale* Rosc. and was first described in the *Shennong's Classic of Materia Medica* (25–220 C.E.). RZ has been used as a food, spice, supplement, flavoring agent, and as an edible herbal medicine, and is characterized by its pungency and aroma, and rich nutrient content with remarkable pharmacological effects.[19,20] As a kind of cash crop, RZ is widely planted and is in huge demand fuelled by a large international trade volume, especially in Arab nations, Burma, China, Japan, India, and other economies.[21] A wide variety of raw or processed forms of RZ are commercially available in the form of spices, condiments, cakes, porridge, and other foods. Modern medicine research has supported the use of RZ as a nutritional dietary supplement or medicine for nausea, upset stomach, diarrhea, arthritis, and rheumatism.[21] It is also used in traditional medicine to treat diseases and symptoms, such as cold, headache, and dysmenorrhea, and as a carminative, antiflatulent, and digestant.[22] Ancient literature and modern studies have demonstrated the anti-inflammatory, bacteriostatic, anti-oxidant, anti-tumour, anti-blood stasis, neuroprotective, and reproductive-system-protective effects of RZ.[23–28] Moreover, in China, a variety of processed products of RZ, such as baked ginger (BG) or ginger charcoal (GC), are used as herbal medicines to meet different clinical needs. The active ingredients responsible for the therapeutic effect of RZ include essential oils (camphene and α-zingiberene), non-volatile compounds (6-gingerol, 8-gingerol, 10-gingerol, gingerol), diphenyl heptane compounds, and other chemical constituents.[19] RZ turns into BG or GC on sand stir-frying, resulting in a change in its constituents. For example, GC possesses higher zingiberene and β-sesquicerin contents than RZ. It also contains α-cypressene, decannl, and γ-eleutherene, which are not found in RZ. Besides, gingerol may turn into gingerols and ginger ketones.[29,30] However, there is a paucity of reports on the molecular mechanism of the therapeutic efficacy of RZ and its processed products (RZPPs, including BG or GC) against PD; moreover, whether the TRP ion channels are involved in this process is not clear.

In the present study, ultrahigh-performance liquid chromatography combined with quadrupole time-of-flight mass spectrometry (UHPLC-Q-TOF MS) was first adopted to analyze the differential quality markers (DQMs) between RZ and RZPPs. Then, a murine model of PD was established using estradiol valerate and oxytocin (EV coupled with OT). Moreover, untargeted metabolomics (UM) was applied to explore the effect of the DQMs on uterine metabolites in a PD mouse model. Furthermore, we investigated whether the molecular mechanism of the therapeutic effect of RZ and RZPPs in the treatment of PD is mediated *via* regulating the TRP ion channel-mediated $ERK_{1/2}$/NF-κB signaling pathway. This study attempts to uncover the scientific connotations of RZ processing and provide a reference for the development of new dietary supplements or medicines.

Materials and methods

Preparation of RZ and RZPPs

RZ was purchased from Shanxi Yuanhetang Chinese Herbal Medicine Co., Ltd (Shanxi, China) and identified as the dry root of *Zingiber officinale* Rosc. by Shuosheng Zhang from Shanxi University of Chinese Medicine. The voucher specimen was deposited in the Herbarium of Shanxi College of Traditional Chinese Medicine (SXTCM), Taiyuan, China (SXTCM-Zhang-2021001).

For BG, RZ was sand stir-fried at 270 °C for approximately 5 min until it became bulged and tanned. It was then placed at room temperature to cool down (unpublished).

For GC, RZ was fried in a pot at 290 °C for approximately 15 min until it turned black on the outside and tanned inside. It was then outfired with water and stored at room temperature to cool down (unpublished).

Preparation of aqueous extracts of RZ and RZPPs

100 g RZ, 100 g BG, and 100 g GC were extracted in a 6-fold volume of distilled water through heating under reflux twice

(1 h each) and then filtered. The filtrate was concentrated under reduced pressure until 1 g mL^{-1}, and aqueous extracts of RZ and RZPPs were stored at 4 °C for *in vivo* experiments. The final yield of aqueous extracts of RZ, BG, and GC were 40.92%, 36.83%, and 30.23%, respectively.

According to the principle and procedure in the *China Pharmacopeia* (2000 edition), the 6-gingerol, 10-gingerol, 6-shogaol, and 8-shogaol content in RZ and RZPPs was determined by high performance liquid chromatography HPLC (U3000, Thermo Fisher Scientific, Waltham, MA, USA), respectively (Fig. S1†).[31] The contents of these four compounds in each herb sample are shown in Table S1.†

UHPLC-Q/TOF-MS

DQMs between RZ and RZPPs were identified based on the method previously used by our team. To analyse the differential uterine metabolites in PD mice treated with RZ and RZPPs, a supernatant of the uterus treated with RZ or RZPPs was obtained and then uploaded to the Agilent 1290 Infinity LC system equipped with a HILIC chromatographic column. Mass spectrometric detection was performed both in positive ion mode (PIM) and negative ion mode (NIM) with electrospray ionization (ESI) using a Triple TOF 6600 mass spectrometer (AB SCIEX).[32–34]

PD modeling and drug administration

Specific pathogen-free (SPF) female BALB/c mice (age: 6–8 weeks; weight: 18 ± 2 g; 4–5 d sexual cycle) were purchased from SiPeiFu, Beijing, China (SCXK-Jing-2019-0010). The mice were allowed to drink water freely and to acclimatize for 1 week in a controlled environment (temperature: 25 ± 2 °C; relative humidity: 55 ± 5%; 12 h/12 h light/dark cycle). All animal procedures followed Animal Research Reporting *In Vivo* Experiments Guidelines (ARRIVE), with the permission of the Ethics Committee of the Shanxi University of Chinese Medicine (permit no. 2021DW676).

After 1 week, the mice were randomly divided into twelve groups (n = 8): normal (blank), control (model), IBF (ibuprofen, 0.12 g kg^{-1} d^{-1}), RZL (low-dose RZ, 0.75 g kg^{-1}), RZM (medium-dose RZ, 1.5 g kg^{-1}), RZH (high-dose RZ, 3 g kg^{-1}), BGL (low-dose BG, 0.75 g kg^{-1}), BGM (medium-dose BG, 1.5 g kg^{-1}), BGH (high-dose BG, 3 g kg^{-1}), GCL (low-dose GC, 0.75 g kg^{-1}), GCM (medium-dose GC, 1.5 g kg^{-1}), and GCH (high-dose GC, 3 g kg^{-1}). Except for the normal mice, mice in the other groups received intragastric administration of EV (0.5 mg kg^{-1}) (J20201038, Bayer Health Care) once daily for 14 consecutive days, and the mice were couple-stimulated using an ice–water mixture (0–4 °C) administered to the lower abdomen once daily (8 min per time) to establish the PD model. On day 6 of modeling, different doses of RZ and RZPP aqueous extracts (as described in the preparation of aqueous extracts of RZ and RZPP section) and IBF were administered by gavage once daily for 10 consecutive days.[35,36] The experimental doses were set based on the following: as stated in the *China Pharmacopeia* (2020 edition), the maximum clinical dose of RZ, BG, and GC for humans is 10 g·60 kg^{-1}. Conventionally, there is a 9.1-fold dose relationship for a mouse compared with a human dosage; therefore, a 1.5 g kg^{-1} dose for mice was converted correspondingly. Considering that the final concentration in the aqueous extracts was 1 g mL^{-1} relative to the original medicinal material, a dose of 1.5 g kg^{-1} of aqueous extracts was used in the present study as the medium dose for the *in vivo* study. The 0.5 and 2 times medium doses were the low and the high doses, respectively.

On day 15, OT (10 U kg^{-1}) (Anhui Hongye Pharmaceutical Co. Ltd, Bengbu, Anhui, China) was administered intraperitoneally. The latency period and frequency of writhing response in mice within 30 min were monitored. After that, the mice were sacrificed. Blood samples were extracted from the abdominal aorta and centrifuged at 4000 rpm and 4 °C for 15 min. Serum samples were collected and preserved in a freezer at −80 °C (DW-HL538, Meling Biomedical, Hefei, Anhui, China). The dorsal root ganglion (DRG) in the lumber 5-sacral 1-segment was instantly extracted. The uterus was isolated and weighed, and the viscera index was calculated (viscera index = organ mass/body mass × 100%).[37] The DRG and uterus were fixed with 4% formaldehyde or stored at −80 °C for further use.

Hematoxylin & eosin (H&E) staining

The uterus was fixed with 4% formaldehyde for 24 h, dehydrated, embedded, and then stained with H&E dye solution according to the standard process. Pathological changes in the uterus were observed by 200× optical microscopy (DM1000; Leica, Wetzlar, HESSEN, Germany).

Enzyme linked immunosorbent assay (ELISA)

Optical density (OD) values of serum estrogen (E_2), progesterone (PROG), $PGF_{2\alpha}$, 6-keto-$PGF_{1\alpha}$, and thromboxane B_2 (TXB_2) were read on a microplate reader (SynergHT, Bio Tek, Vermont, New England, USA) using corresponding ELISA kits (no. 2021091021, 2021091698, 2021092315, 2021091908, 2021092259; Shanghai Enzyme-linked, Shanghai, China).

Western blotting

Total proteins of the DRG and uterine tissues were obtained using T-PER tissue protein extraction reagent. The Bradford method was adopted to examine protein concentration. SDS-PAGE was performed to obtain 30 μg of proteins, which were then transferred to a nitrocellulose membrane. The membrane was blocked at room temperature for 2 h, followed by overnight incubation with primary antibodies, including TRPV1, TRPM8, CaMKII, p-$ERK_{1/2}$/$ERK_{1/2}$, p-NF-κB (p65)/NF-κB (p65), p-$I\kappa B_\alpha$/$I\kappa B_\alpha$, COX-2, and β-actin (ABclonal Technology Co. Ltd, Wuhan, China) at 4 °C. TBST washing was performed. Subsequently, secondary antibodies of HRP-conjugated goat anti-rabbit IgG (BST16E18B16E55, Boster Technology Co. Ltd, Wuhan, China) were added at room temperature for 4 h. Protein bands were developed by a GeneGnome system (GeneGnome XRQ, Gene, USA) and analyzed by ImageJ (ImageJ2, NIH, USA) according to the grey value.[38]

Immunohistochemistry (IHC)

TRPV1, TRPM8, and COX-2 expressions were visualized using immunohistochemistry. For antigen retrieval, 0.1% trypsin was used to digest sections at 37 °C for 30 min. Then tissues were incubated overnight with primary antibody against mice TRPV1 (1 : 200), TRPM8 (1 : 200) or COX-2 (1 : 200) at 4 °C, followed by labelling with biotinylated horseradish peroxidase (HRP)-conjugated secondary antibody for 30 min at 37 °C and detection using a diaminobenzidine chromogen. Photographs were obtained with a microscope system (DM1000; Leica, Wetzlar, HESSEN, Germany) at a magnification of 400×.[33] ImageScope software (Leica Biosystems, Wetzlar, HESSEN, Germany) was used to identify and analyze the strongly-positive, moderately-positive, weakly-positive, and negative stained areas (in pixels) in each IHC image, and the percentage positive staining was calculated. Strongly-positive, moderately-positive, weakly-positive, and negative stained areas in tissue sections were labeled as dark brown, brown yellow, light yellow, and blue, respectively. The H-score was calculated for semi-quantification of tissue staining using the following formula: H-score = $\sum$(PI × I) = (percentage of cells of weak intensity × 1) + (percentage of cells of moderate intensity × 2) + (percentage of cells of strong intensity × 3), where PI is the percentage of positive cells among all cells in the section, and I stands for color intensity.[39,40]

Statistical analysis

Data processing for LC-MS/MS. Data from UHPLC-Q/TOF-MS were processed by principal component analysis (PCA) and orthogonal partial least-squares discriminant analysis (OPLS-DA). DQMs or DMs were identified by VIP > 1 or VIP > 2 and P < 0.05. The MetaboAnalyst 5.0 database was used to perform metabolic pathway enrichment analysis.[33]

Statistical analysis. Data are presented as mean ± standard error of mean (SEM) from three independent experiments. Differences between groups were assessed using one-way analysis of variance (ANOVA) with a *post hoc* Tukey test in GraphPad Prism (version 5.0; GraphPad Software, La Jolla, CA, USA). P values <0.05 were considered indicative of statistical significance.

Results

DQMs between RZ and RZPPs

Total ion chromatograms (TIC) of QC samples were obtained and aligned. The response intensity and retention time between each chromatographic peak were basically overlapping (Fig. 1A). A total of 1591 and 927 quality markers in the PIM and NIM were obtained, respectively. Based on univariate analysis, the differential metabolites with fold change (FC) > 1.5 or FC < 0.67 and P value <0.05 in positive ion mode are visually displayed in the form of a volcanic map (Fig. 1B and C). The results of PCA demonstrated significant separation of the samples with RZ and RZPPs (Fig. 1D). To minimize the effects of other independent variables caused by the difference in chemical components between RZ and RZPPs, OPLS-DA was performed. The OPLS-DA model was able to distinguish two sets of samples (Fig. 1E and G). The results of permutation testing showed that the R^2 and Q^2 of the random model reduced with a decrease of replacement retention, indicating good model stability without overfitting issues (Fig. 1F and H) (Fig. S2†).

According to VIP > 2 in OPLS-DA and P < 0.05, there were 40 DQMs between RZ and BG in the PIM, including 12 up-regulated markers and 28 down-regulated markers. Between BG and GC, there were 43 DQMs, including 15 up-regulated markers and 28 down-regulated markers, which were mainly involved in benzenoids (such as [6]-gingerol) and lipids and lipidoids (such as (+)-carvone) (Tables S2 and S3†). Correlation analysis revealed that 2-methyl-*n*-(4-methylphenyl)alanine and Pyroglu-phe were the two DQMs that showed the most positive correlation with other markers, while 2,5-di-*tert*-butylaniline and Val-Ala, 5.beta.-pregnane-3.alpha.,17,21-triol-11,20-dione and Phe-pro showed the most negative correlation with other markers (Fig. 1I and J).

Effect of RZ and RZPPs on pathological signs in PD mice

The latency period of writhing response, uterus index, and pathological manifestations of the uterus were analysed and recorded to study the effects of RZ and RZPPs on pathological signs in PD mice.

As compared to the normal group, the uterus index in the control group was significantly higher (P < 0.0001). After drug administration, the latency period of writhing response was significantly prolonged (BGL, P < 0.05; RZL, RZM, GCL, GCM, P < 0.01; IBF, P < 0.0001) while the uterus index was significantly decreased (RZL, BGL, BGM, P < 0.05; GCL, GCH, P < 0.01; GCM, P < 0.001; IBF, P < 0.0001), as compared to the control group. When compared to the RZL group, the uterus index was much lower in the GCM group (P < 0.05) and the IBF group (P < 0.001) (Fig. 2A and B).

In addition, drug administration led to varying degrees of decrease in uterine volume (Fig. 2C), accompanied by thinning of uterine smooth muscle, a smaller number of inflammatory cells, and relatively normal cell arrangement (Fig. 2D).

RZ and RZPPs decrease serum E_2, $PGF_{2\alpha}$, TXB_2 but increase PROG and 6-keto-$PGF_{1\alpha}$ in PD mice

Enzyme linked immunosorbent assay (ELISA) was used to determine the serum levels of estrogen (E_2), progesterone (PROG), $PGF_{2\alpha}$, 6-keto-$PGF_{1\alpha}$, and thromboxane B_2 (TXB_2) in PD mice.

As compared to the normal group, the serum levels of E_2 (P < 0.001), $PGF_{2\alpha}$ (P < 0.01), and TXB_2 (P < 0.01) were significantly increased in the control group, while the serum levels of PROG (P < 0.01) and 6-keto-$PGF_{1\alpha}$ (P < 0.0001) were significantly decreased.

After treatment, the serum levels of E_2 (RZL, RZH, BGM, GCL, P < 0.05; IBF, RZM, GCH, P < 0.01), $PGF_{2\alpha}$ (IBF, BGM, BGH, GCH, P < 0.05; RZM, RZH, P < 0.01), TXB_2 (IBF, BGH,

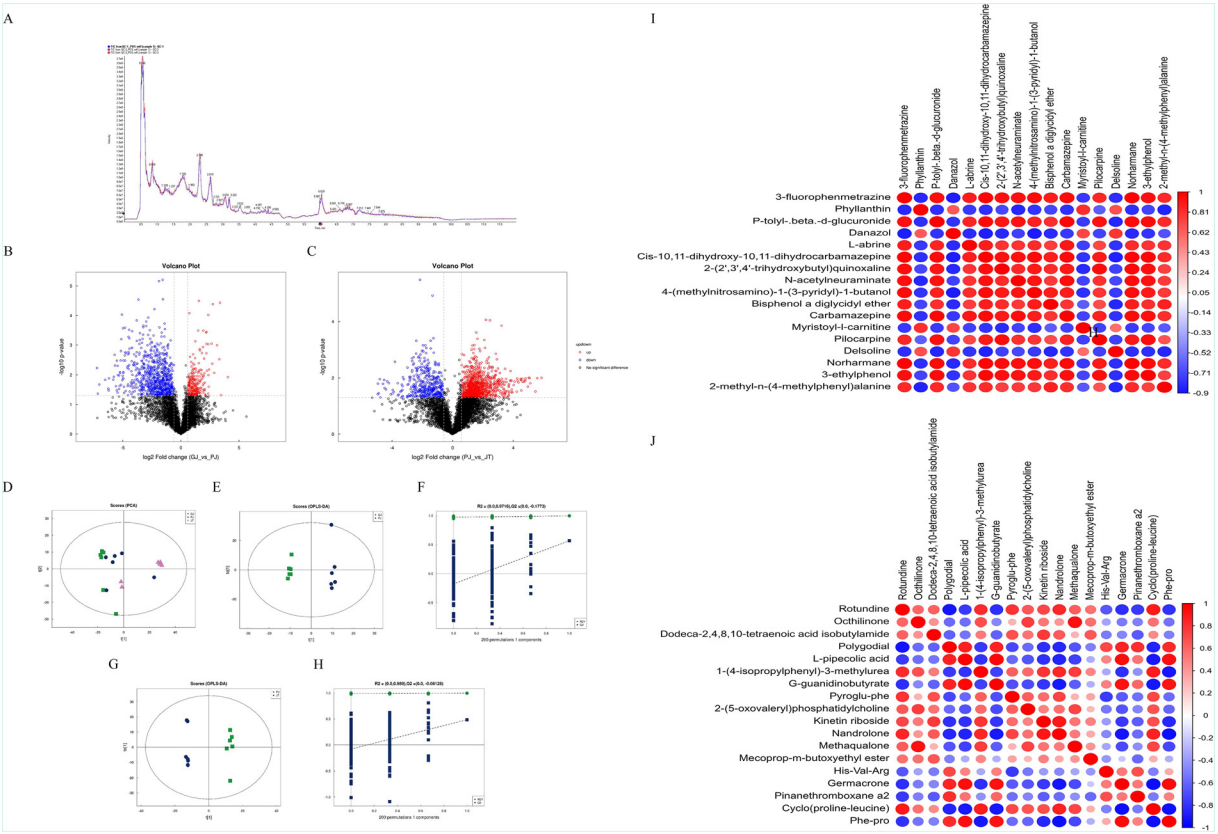

Fig. 1 The DQMs between RZ and RZPPs. (A) Total ion chromatograms in the positive ion mode. (B) Volcano plots between RZ and BG in positive ion mode. (C) Volcano plots between BG and GC in positive ion mode. (D) PCA score plot for each group in positive ion mode. (E) OPLS-DA score plots between RZ and BG in positive ion mode. (F) 200-Time permutations were performed and plotted between RZ and BG in positive ion mode. (G) OPLS-DA score plots between BG and GC in positive ion mode. (H) 200-Time permutations were performed and plotted between BG and GC in positive ion mode. (I) Heat map exhibiting intensities of DQMs between RZ and BG in positive ion mode. (J) Heat map exhibiting intensities of DQMs between BG and GC in positive ion mode.

GCM, $P < 0.05$), PROG (IBF, GCH, $P < 0.01$) and 6-keto-$PGF_{1\alpha}$ (IBF, BGL, BGH, GCM, $P < 0.05$; BGM, $P < 0.01$; GCL, GCH, $P < 0.001$) exhibited a conversely changing trend.

Additionally, as compared to the RZM group, the PROG level was significantly increased in the IBF and GCH groups (both $P < 0.01$) and 6-keto-$PGF_{1\alpha}$ was significantly increased in the GCH group ($P < 0.05$). As compared to the RZH group, PROG and 6-keto-$PGF_{1\alpha}$ were remarkably higher in the GCH group (both $P < 0.05$) (Fig. 2E).

Effects of RZ and RZPPs on uterine metabolic profiles in PD mice

According to VIP > 2 in OPLS-DA and $P < 0.05$, the differential uterine metabolites were mainly involved in benzenoids, organic acids and derivatives (Table S4) (Fig. S3†). Enrichment analysis revealed 31 differential metabolic pathways between the normal and control groups, mainly including an amino acid metabolism pathway, a protein metabolism pathway, an energy metabolism pathway, a lipid metabolism pathway, and a neuron-associated metabolism pathway. Of note, the TRP ion channels were different between the two groups, indicating that the inflammatory mediator regulation of TRP channels was a potential therapeutic target in the treatment of PD (Fig. 3A and B). Furthermore, as compared to the control group, there was mainly one differential metabolic pathway (for histidine metabolism) in the RZ group, nine differential metabolic pathways (D-arginine and D-ornithine metabolism, central carbon metabolism in cancer and protein digestion and absorption) in the BG group, and five differential metabolic pathways (sphingolipid metabolism, cAMP signalling pathway, mineral absorption, pentose phosphate pathway and central carbon metabolism in cancer) in the GC groups (Fig. 3C and D).

Associations between DQMs and DMs

R version 4.2.0 (https://cran.r-project.org/) was used to construct a correlation network of DQMs and DMs in the uterine tissue of PD mice (Fig. 3E and F). DQMs of RZ and BG, leukotriene.e4, showed the strongest correlation with its uterine differential metabolite, urocanate. DQMs of BG and GC, 2-butoxypyridine, showed the strongest correlation with its uterine differential metabolite, fenpropidin.

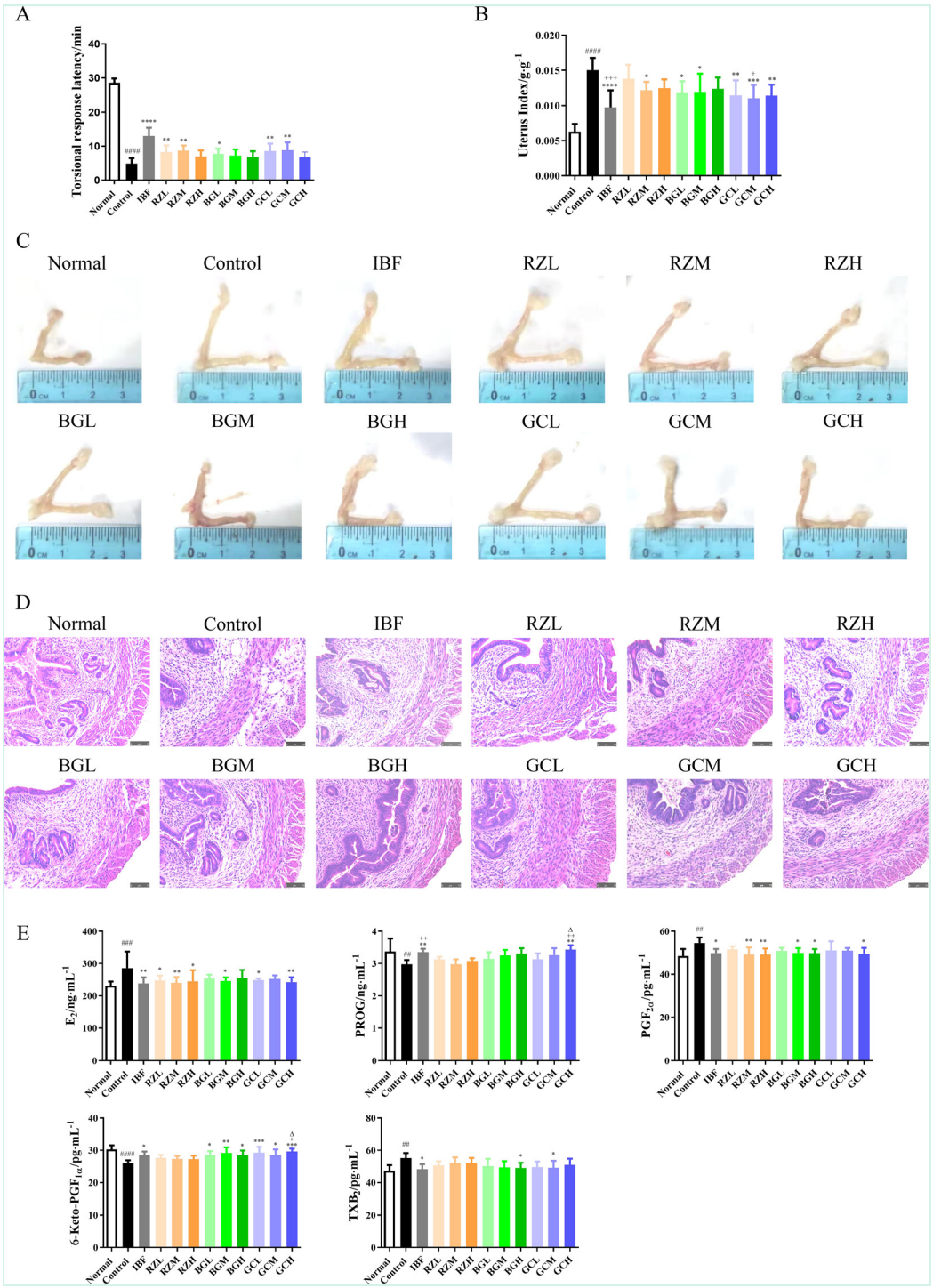

Fig. 2 RZ and RZPPs alleviate the pathological signs of PD mice. PD was induced in mice using estradiol valerate coupled with oxytocin, and then the efficacy of RZ and RZPPs was observed. The latency period of writhing response (A), uterus index (B), uterine tissue morphology (C), and pathological changes of the uterus (hematoxylin & eosin staining, 200×) (D) were observed or calculated. Concentrations of E_2, PROG, $PGF_{2\alpha}$, 6-keto-$PGF_{1\alpha}$ and TXB_2 were determined by ELISA (E). Normal: blank, control: model, IBF: ibuprofen, RZL: low-dose RZ, RZM: medium-dose RZ, RZH: high-dose RZ, BGL: low-dose BG, BGM: medium-dose BG, BGH: high-dose BG, GCL: low-dose GC, GCM: medium-dose GC, GCH: high-dose GC. $^{\#\#\#\#}P < 0.0001$ *vs.* normal group. $^{*}P < 0.05$, $^{**}P < 0.01$, $^{***}P < 0.001$, $^{****}P < 0.0001$ *vs.* control group. $^{+}P < 0.05$, $^{++}P < 0.01$, $^{+++}P < 0.001$ *vs.* RZL group. $^{\Delta}P < 0.05$ *vs.* RZH group.

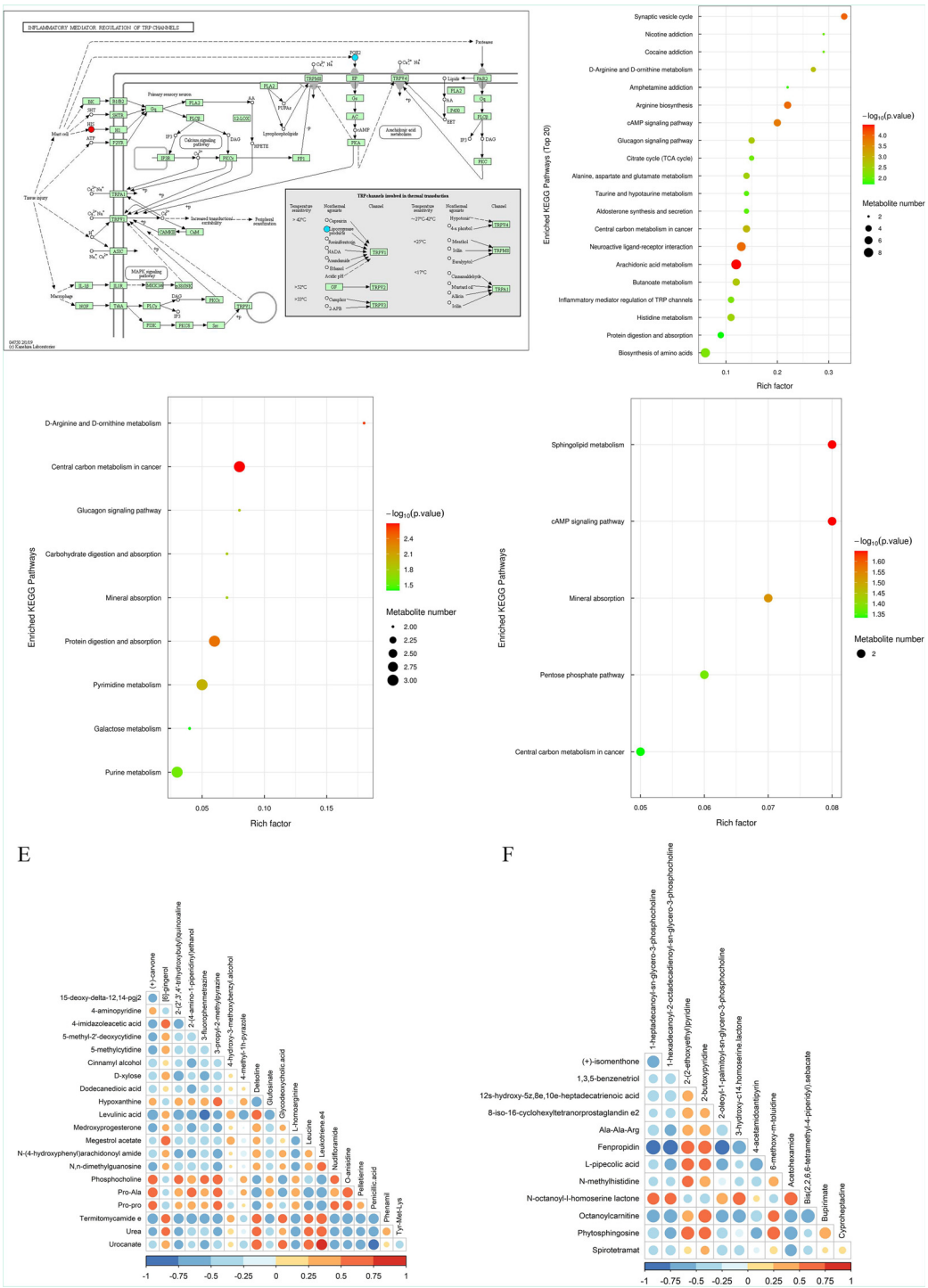

Fig. 3 UM and correlation analyses. TRP signaling pathway (A) (https://www.kegg.jp/kegg-bin/show_pathway?mmu04750+C04742); KEGG pathway enrichment analyses of normal and control (B), BG and control (C), GC and control (D); the correlation network of DQMs of RZ and BG and DMs in PD mouse uterus (E), DQMs of BG and GC and DMs in PD mouse uterus (F).

RZ and RZPPs significantly elevate the expression levels of TRPV1, p-IκB$_\alpha$/IκB$_\alpha$ and reduce the expression levels of TRPM8, CaMKII, p-ERK$_{1/2}$/ERK$_{1/2}$, p-NF-κB (p65)/NF-κB (p65) and COX-2

To study the underlying mechanism of the action of RZ and RZPPs, western blotting was used to determine the protein levels of TRPV1, TRPM8, CaMKII, p-ERK$_{1/2}$/ERK$_{1/2}$, p-NF-κB (p65)/NF-κB (p65), p-IκB$_\alpha$/IκB$_\alpha$ and COX-2 in the uteri of PD mice, and the protein levels of TRPV1 and TRPM8 in the DRG of PD mice.

The levels of TRPV1 ($P < 0.0001$) and p-IκB$_\alpha$/IκB$_\alpha$ ($P < 0.001$) in the control group were significantly reduced compared to those in the normal group, but the levels of TRPM8 ($P < 0.01$),

CaMKII ($P < 0.001$), p-ERK$_{1/2}$/ERK$_{1/2}$ ($P < 0.01$), p-NF-κB (p65)/NF-κB (p65) ($P < 0.01$) and COX-2 ($P < 0.01$) were conversely elevated.

After drug administration, the levels of TRPV1 (IBF, $P < 0.05$; GCM, GCH, $P < 0.01$) and p-IκB$_\alpha$/IκB$_\alpha$ (GCH, $P < 0.05$) were significantly increased. In contrast, the levels of TRPM8 (RZL, RZM, GCL, $P < 0.05$; IBF, BGL, BGM, GCH, $P < 0.01$), CaMKII (IBF, $P < 0.05$; RZH, BGM, $P < 0.01$; BGL, $P < 0.001$), p-ERK$_{1/2}$/ERK$_{1/2}$ (RZM, BGH, $P < 0.05$; IBF, RZL, BGL, GCM, GCH, $P < 0.01$), p-NF-κB (p65)/NF-κB (p65) (IBF, RZH, GCH, $P < 0.01$) and COX-2 (IBF, RZH, BGM, BGH, GCL, GCM, $P < 0.05$; RZM, GCH, $P < 0.01$) were profoundly decreased (Fig. 4A).

The levels of TRPV1 ($P < 0.001$) in the control group were significantly reduced compared to the levels in the normal group, but the levels of TRPM8 ($P < 0.01$) were conversely elevated.

After drug administration, the levels of TRPV1 (IBF, $P < 0.05$; RZH, $P < 0.01$) were significantly increased. In contrast, the levels of TRPM8 (RZL, RZM, RZH, BGH, $P < 0.05$; IBF, $P < 0.01$) were profoundly decreased (Fig. 4B).

Consistently, the results of IHC showed that the levels of TRPV1 ($P < 0.001$) in the control group were significantly reduced compared to those in the normal group, and the levels of TRPM8 ($P < 0.001$) and COX-2 ($P < 0.01$) were remarkably elevated. After drug administration, the results of the IHC

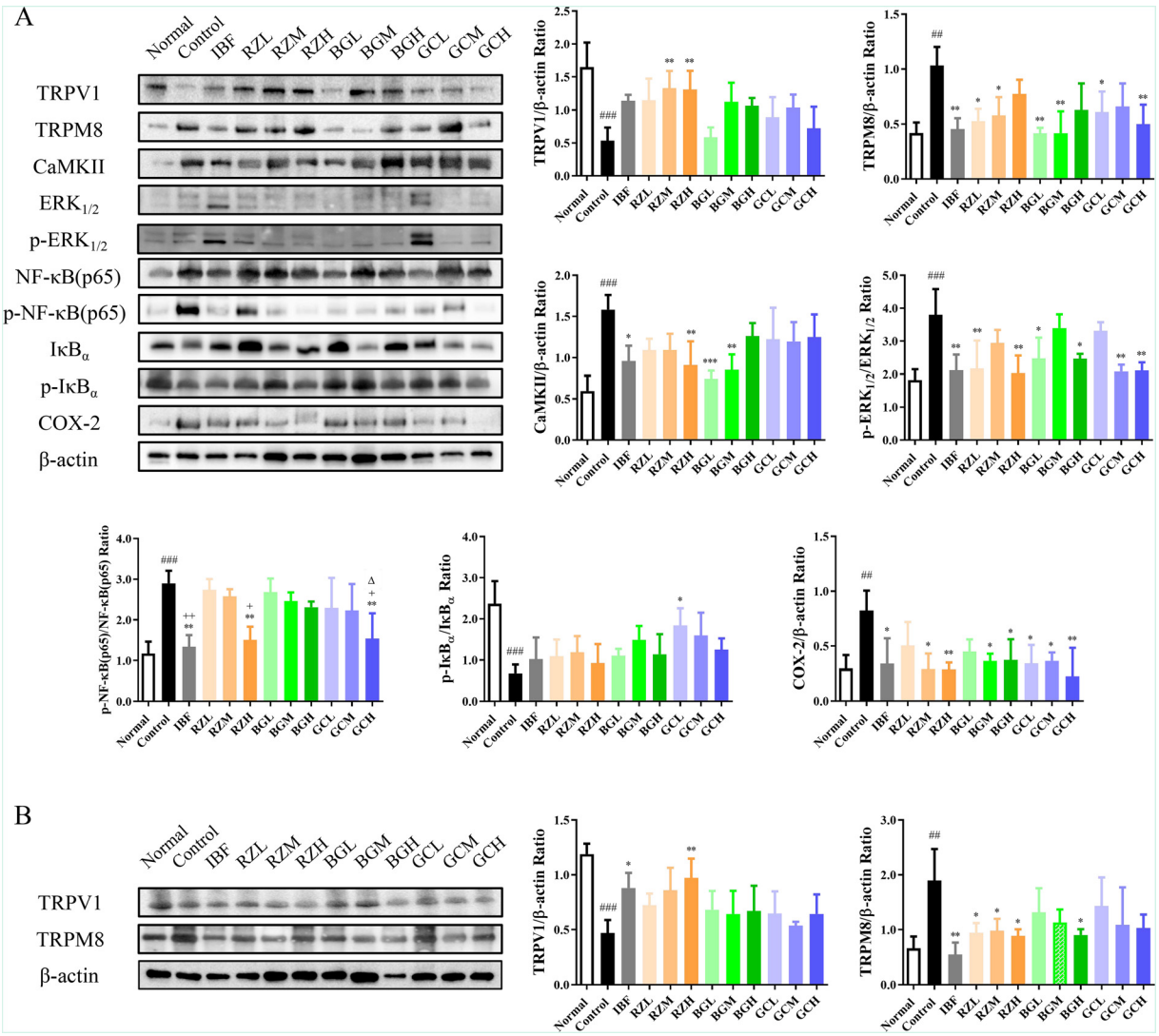

Fig. 4 RZ and RZPPs can significantly affect TRPV1, TRPM8 and ERK$_{1/2}$/NF-κB signaling pathway protein expression levels in the uteri and DRG of PD mice. The expression levels in the uteri (A) and in the DRG (B) of PD mice were detected by western blotting, and their expression was normalized relative to β-actin. Each band was presented as a representative figure, and a histogram was calculated from the band density value of at least three independent experiments. β-Actin was used as an internal control. Data are presented as mean ± SD for each group ($n = 3$). $^{\#\#}P < 0.01$, $^{\#\#\#}P < 0.001$ *vs.* normal group. Normal: blank, control: model, IBF: ibuprofen, RZL: low-dose RZ, RZM: medium-dose RZ, RZH: high-dose RZ, BGL: low-dose BG, BGM: medium-dose BG, BGH: high-dose BG, GCL: low-dose GC, GCM: medium-dose GC, GCH: high-dose GC. $^{*}P < 0.05$, $^{**}P < 0.01$ *vs.* control group. $^{+}P < 0.05$, $^{++}P < 0.01$ *vs.* RZL group. $^{\Delta}P < 0.05$ *vs.* BGL group.

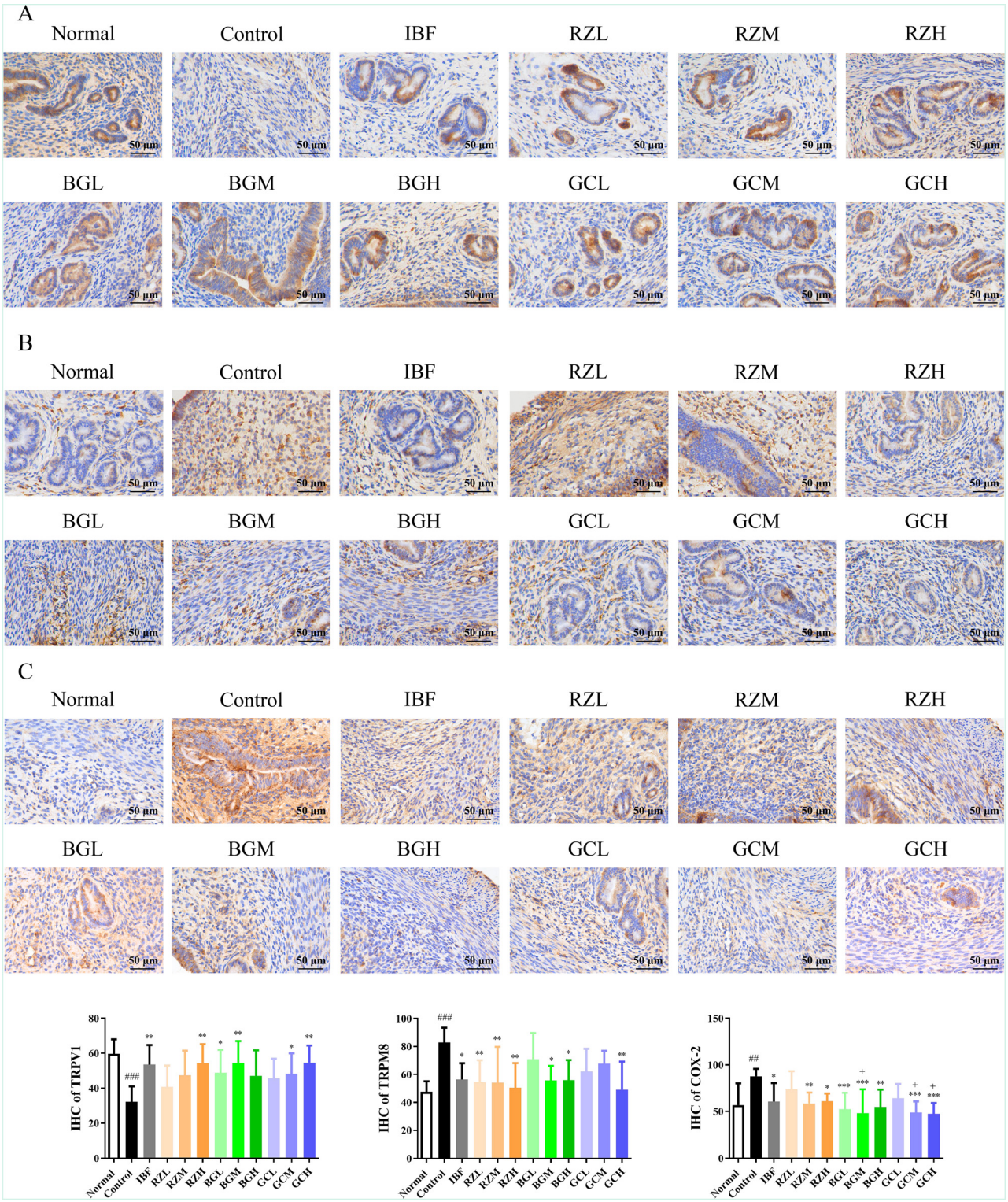

Fig. 5 Immunohistochemistry analysis. The TRPV1 (A), TRPM8 (B) and COX-2 (C) expressions were detected by immunohistochemical analysis (400×). Normal: blank, control: model, IBF: ibuprofen, RZL: low-dose RZ, RZM: medium-dose RZ, RZH: high-dose RZ, BGL: low-dose BG, BGM: medium-dose BG, BGH: high-dose BG, GCL: low-dose GC, GCM: medium-dose GC, GCH: high-dose GC. $^{\#\#}P < 0.01$, $^{\#\#\#}P < 0.001$, $^{\#\#\#\#}P < 0.0001$ *vs.* normal group. $^{*}P < 0.05$, $^{**}P < 0.01$, $^{***}P < 0.001$ *vs.* control group. $^{+}P < 0.05$ *vs.* RZL group.

showed that the levels of TRPV1 (BGL, GCM, $P < 0.05$; IBF, RZH, BGM, GCH, $P < 0.01$) were significantly increased. The levels of TRPM8 (IBF, BGM, BGH, $P < 0.05$; RZL, RZM, RZH, GCH, $P < 0.01$) and COX-2 (IBF, RZH, $P < 0.05$; RZM, BGH, $P < 0.01$; BGL, BGM, GCM, GCH, $P < 0.001$) were remarkably reduced (Fig. 5).

Discussion

TRP ion channels are closely involved in the sensation of temperature and pain. TRPV1 and TRPM8 channel proteins play important roles in the onset and development of PD. TRPV1 regulates pain signals under the mediation of PKA and PKB, produced by the sensitization effect of inflammatory molecules (such as bradykinin), Ca^{2+}/CaMKII, and arachidonic acid metabolites.[11] In addition, TRPV1 can aggravate pain or induce hyperalgesia after sensitization with other pro-inflammatory mediators (such as PGs) *via* activation of the PI3K and ERK pathways.[41,42] TRPM8 can be cold-activated to increase heat production, thereby maintaining an ambient temperature in the body.[43,44] Activated TRPV1 and TRPM8 can increase the intracellular Ca^{2+} content while the activated Ca^{2+}/CaMKII can subsequently elevate the expression of downstream $ERK_{1/2}$ to mediate an oxytocin signal and regulate the production of inflammatory cytokines.[45–47] Phosphorylated ERK can affect the phosphorylation of $I\kappa B_\alpha$, an important indicator of the activation of the NF-κB pathway, which in turn can induce the aberrant activation of some key proteins, such as p65.[48] Phosphorylated NF-κB can induce the expression of COX-2 and limit the rate of transformation of arachidonic acid to PGs.[49] $PGF_{2\alpha}$, PGI_2, and TXA_2 are PGs with biological activities produced by the human uterus. Given the relatively short half-life of PGI_2 and TXA_2, their stable metabolites, TXB_2 and 6-keto-$PGF_{1\alpha}$, are commonly used as markers of PGs in the uterus. It has been established that PROG promotes the synthesis of PGs in endometrium, stimulates uterine smooth muscle contraction, and subsequently aggravates pain sensations. Under the guidance of TCM theory, traditional herbal medicines are processed by traditional pharmaceutical technology according to the needs of clinical medication and the nature of drugs, which can play a role in modifying drug properties, reducing toxicity, and improving the curative effect.[50–52] RZ and RZPPs are commonly used to alleviate PD, which has been proven by modern pharmacological research.[53–56] A study by Kim *et al.* suggested that the antioxidant effects of ginger extract and its pungent constituents were mediated through TRPC5 and TRPA1.[57] Yang *et al.* found that gingerol derived from ginger may improve digestive function by stimulating secretion from endocrine cells of the gut by inducing TRPA1-mediated calcium influx.[58] These findings suggest that ginger and its constituents can regulate TRP channels. However, whether the TRP ion channels are involved in mediating the therapeutic effect of RZ and RZPPs in PD has rarely been reported. To the best of our knowledge, this is the first study to verify that the therapeutic effect of RZ and RZPPs against PD is mediated *via* regulation of the TRP ion channels-mediated $ERK_{1/2}$/NF-κB signaling pathway, and it provides a reference for the development of new dietary supplements or medicines.

In the present study, UM was applied to prove that RZ and RZPPs alleviated pain in PD mice by regulating the TRP ion channels. Both medicines were found to ameliorate the pathological changes of PD, including increased secretion from endometrial glands, extensive infiltration of inflammatory cells and edema, uterine smooth muscle thickening, cellular hypertrophy, and disordered arrangements. In addition, RZ and RZPPs decreased the serum levels of E_2, $PGF_{2\alpha}$, TXB_2, but increased the levels of PROG and 6-keto-$PGF_{1\alpha}$ in PD mice. The results of UM showed that the DMs of the normal group and the control group were enriched in the inflammatory mediator regulation of TRP channels, indicating a certain correlation between the TRP channels and PD. Therefore, from the perspective of TRP channel proteins, WB and IHC were used to detect protein expression levels of the TRP ion channel-mediated $ERK_{1/2}$/NF-κB signaling pathway. The results showed remarkably elevated levels of TRPV1, p-$I\kappa B_\alpha$/$I\kappa B_\alpha$ and reduced levels of TRPM8, CaMKII, p-$ERK_{1/2}$/$ERK_{1/2}$, p-NF-κB (p65)/NF-κB (p65) and COX-2 after treatment. Admittedly, there were other enriched pathways between each treatment group and the control group; therefore, further research is necessary.

The present study also identified crossovers between RZ and BG, while there was a distinct discrimination between RZ and GC. We reasoned that during processing, the chemical components of RZ change with increasing temperatures and time extensions. This study also established a connective network between the DQMs and the uterine metabolic pathways in PD mice. Due to the limited availability of experimental samples and inter-individual differences, there was no significant dose-dependence of RZ and RZPPs, but we did observe a treatment trend. Therefore, further research is required to support this theory and to enable in-depth characterization of the mechanism of action.

Conclusions

To conclude, RZ and RZPPs can improve the pathological status and pain in estradiol valerate coupled with oxytocin-induced dysmenorrhea *via* regulating the TRP ion channel-mediated $ERK_{1/2}$/NF-κB signaling pathway.

Abbreviations

ANOVA	Analysis of variance
ARRIVE	Animal research reporting *in vivo* experiments guidelines
BG	Baked ginger
Ca^{2+}	Calcium
CaMKII	Calmodulin-dependent protein kinase II
COX-2	Cyclooxygenase-2
DMs	Differential metabolomics

DQMs	Differential quality markers
DRG	Dorsal root ganglion
E_2	Estrogen
$ERK_{1/2}$	Extracellular regulated protein kinases$_{1/2}$
ESI	Electrospray ionization
EV	Estradiol valerate
GC	Ginger charcoal
H&E	Hematoxylin & eosin
IHC	Immunohistochemistry
NF-κB	Nuclear factor-κB
NIM	Negative ion mode
NSAID	Non-steroidal anti-inflammatory drugs
OPLS-DA	Orthogonal partial least-squares discriminant analysis
OT	Oxytocin
PCA	Principal component analysis
PD	Primary dysmenorrhea
PG	Prostaglandin
$PGF_{2\alpha}$	Prostaglandin $F_{2\alpha}$
PIM	Positive ion mode
PROG	Progesterone
RZ	Rhizoma zingiberis, ginger
RZPPs	Rhizoma zingiberis processed products
SPF	Specific pathogen-free
TCM	Traditional Chinese medicine
TIC	Total ion chromatograms
TRP	Transient receptor potential
TXB_2	Thromboxane B_2
UHPLC-Q-TOF MS	Ultra high-performance liquid chromatography combined with quadrupole time-of-flight mass spectrometry
UM	Untargeted metabolomics

Ethical statement

The animal study protocol was approved by the Animal Care and Use Committee of Shanxi University of Chinese Medicine (approval number: 2021DW676).

Author contributions

All authors contributed extensively to the refinement of the study protocol. Conceptualization, X. L., X. M. and S. Z.; methodology, X. L. and X. M.; investigation, X. S. and K. R.; resources, S. Z.; data curation, X. L. and X. M.; writing – original draft preparation, X. L. and X. M.; writing – review and editing, X. L. and X. M.; supervision, X. Q.; project administration, C. N. All authors have read and agreed to the published version of the manuscript.

Conflicts of interest

There are no conflicts to declare.

Acknowledgements

This work was funded by the project of Shanxi Key Laboratory of Traditional Herbal Medicines Processing (no. 202104010910029), the Innovation Team of Shanxi University of Chinese Medicine (no. 2022TD1014) and the Discipline Construction of Shanxi University of Chinese Medicine (no. 2018-01).

References

1 M. Kazama, K. Maruyama and K. Nakamura, Prevalence of dysmenorrhea and its correlating lifestyle factors in Japanese female junior high school students, *Tohoku J. Exp. Med.*, 2015, **236**, 107–113.
2 Z. Hu, L. Tang, L. Chen, A. C. Kaminga and H. Xu, Prevalence and Risk Factors Associated with Primary Dysmenorrhea among Chinese Female University Students: A Cross-sectional Study, *J. Pediatr. Adolesc. Gynecol.*, 2020, **33**, 15–22.
3 S. Iacovides, I. Avidon and F. C. Baker, What we know about primary dysmenorrhea today: a critical review, *Hum. Reprod. Update*, 2015, **21**, 762–778.
4 E. Ferries-Rowe, E. Corey and J. S. Archer, Primary Dysmenorrhea: Diagnosis and Therapy, *Obstet. Gynecol.*, 2020, **136**, 1047–1058.
5 N. Li, J. Li and P. Gai, Effects of Modified Wenjing Decoction Combined with Online Publicity and Education on the Treatment of Primary Dysmenorrhea of Cold Coagulation and Blood Stasis, *J. Healthcare Eng.*, 2022, **2022**, 1899356.
6 L. G. Nisembaum, G. Loentgen, T. L'Honoré, P. Martin, C. H. Paulin, M. Fuentès, K. Escoubeyrou, M. J. Delgado, L. Besseau and J. Falcón, Transient Receptor Potential-Vanilloid (TRPV1-TRPV4) Channels in the Atlantic Salmon, Salmo salar. A Focus on the Pineal Gland and Melatonin Production, *Front. Physiol.*, 2021, **12**, 784416.
7 Y. C. Xu, Y. Zhu, Z. H. Li, F. F. Hao and X. P. Wang, Effects of Jingshu Granules on TRPV1, TRPM8 and related inflammatory factors in primary dysmenorrhea rats, *Lishizhen Med. Mater. Med. Res.*, 2020, **31**, 1322–1324.
8 C. Montell, The TRP superfamily of cation channels, *Sci. STKE*, 2005, **2005**, re3.
9 J. Nie, X. Liu and S. W. Guo, Immunoreactivity of oxytocin receptor and transient receptor potential vanilloid type 1 and its correlation with dysmenorrhea in adenomyosis, *Am. J. Obstet. Gynecol.*, 2010, **202**, 346.
10 J. Xu, Y. Xu, Y. Zhu, Z. Li and X. Wang, Molecular Targets and Associated Signaling Pathways of Jingshu Granules in Ovarian Cysts Based on Systemic Pharmacological Analysis, *BioMed Res. Int.*, 2021, **2021**, 6660087.
11 M. Duitama, Y. Moreno, S. P. Santander, Z. Casas, J. J. Sutachan, Y. P. Torres and S. L. Albarracín, TRP Channels as Molecular Targets to Relieve Cancer Pain, *Biomolecules*, 2021, **12**.

12 F. A. Fajrin, A. E. Nugroho, A. Nurrochmad and R. Susilowati, Ginger extract and its compound, 6-shogaol, attenuates painful diabetic neuropathy in mice via reducing TRPV1 and NMDAR2B expressions in the spinal cord, *J. Ethnopharmacol.*, 2020, **249**, 112396.

13 Y. Yin, M. Wu, L. Zubcevic, W. F. Borschel, G. C. Lander and S. Y. Lee, Structure of the cold- and menthol-sensing ion channel TRPM8, *Science*, 2018, **359**, 237–241.

14 X. Gao, J. Zhuang, L. Zhao, W. Wei and F. Xu, Cross-effect of TRPV1 and EP3 receptor on coughs and bronchopulmonary C-neural activities, *PLoS One*, 2021, **16**, e0246375.

15 C. Xue, S. X. Liu, J. Hu, J. Huang, H. M. Liu, Z. X. Qiu and F. Huang, Corydalis saxicola Bunting total alkaloids attenuate paclitaxel-induced peripheral neuropathy through PKCε/p38 MAPK/TRPV1 signaling pathway, *Chin. Med.*, 2021, **16**, 58.

16 C. Li, L. Xu, X. Lin, Q. Li, S. Liu, L. Fan, W. Fu, F. Liu, Z. Yuan and G. Qin, Network Pharmacology and Molecular Docking Verify the Mechanism of Qinshi Simiao San in Treating Chronic Prostatitis in the Rat Model, *J. Evidence-Based Complementary Altern. Med.*, 2022, **2022**, 7098121.

17 H. Jiang, G. M. Ashraf, M. Liu, K. Zhao, Y. Wang, L. Wang, J. Xing, B. S. Alghamdi, Z. Li and R. Liu, Tilianin Ameliorates Cognitive Dysfunction and Neuronal Damage in Rats with Vascular Dementia via p-CaMKII/ERK/CREB and ox-CaMKII-Dependent MAPK/NF-κB Pathways, *Oxid. Med. Cell. Longevity*, 2021, **2021**, 6673967.

18 V. May, T. A. Clason, T. R. Buttolph, B. M. Girard and R. L. Parsons, Calcium influx, but not intracellular calcium release, supports PACAP-mediated ERK activation in HEK PAC1 receptor cells, *J. Mol. Neurosci.*, 2014, **54**, 342–350.

19 R. Kiyama, Nutritional implications of ginger: chemistry, biological activities and signaling pathways, *J. Nutr. Biochem.*, 2020, **86**, 108486.

20 A. Hajihassani, W. Ye and B. B. Hampton, First report of Meloidogyne javanica on Ginger and Turmeric in the United States, *J. Nematol.*, 2019, **51**, 1–3.

21 K. Tanaka, M. Arita, H. Sakurai, N. Ono and Y. Tezuka, Analysis of chemical properties of edible and medicinal ginger by metabolomics approach, *BioMed Res. Int.*, 2015, **2015**, 671058.

22 M. S. Baliga, R. Haniadka, M. M. Pereira, J. J. D'Souza, P. L. Pallaty, H. P. Bhat and S. Popuri, Update on the chemopreventive effects of ginger and its phytochemicals, *Crit. Rev. Food Sci. Nutr.*, 2011, **51**, 499–523.

23 M. Y. Song, D. Y. Lee, S. Y. Park, S. A. Seo, J. S. Hwang, S. H. Heo and E. H. Kim, Erratum: Steamed Ginger Extract Exerts Anti-inflammatory Effects in Helicobacter pylori-infected Gastric Epithelial Cells through Inhibition of NF-κB, *J. Cancer Prev.*, 2022, **27**, 77.

24 H. Li, R. Rafie, Z. Xu and R. A. Siddiqui, Phytochemical profile and anti-oxidation activity changes during ginger (Zingiber officinale) harvest: Baby ginger attenuates lipid accumulation and ameliorates glucose uptake in HepG2 cells, *Food Sci. Nutr.*, 2022, **10**, 133–144.

25 A. Farmoudeh, A. Shokoohi and P. Ebrahimnejad, Preparation and Evaluation of the Antibacterial Effect of Chitosan Nanoparticles Containing Ginger Extract Tailored by Central Composite Design, *Adv. Pharm. Bull.*, 2021, **11**, 643–650.

26 M. A. Abdel-Rasol, N. M. El-Beih, S. S. Yahya and W. M. El-Sayed, The Antitumor Activity of Ginger against Colorectal Cancer Induced by Dimethylhydrazine in Rats, *Anti-Cancer Agents Med. Chem.*, 2022, **22**, 1601–1610.

27 M. Su, G. Cao, X. Wang, R. Daniel, Y. Hong and Y. Han, Metabolomics study of dried ginger extract on serum and urine in blood stasis rats based on UPLC-Q-TOF/MS, *Food Sci. Nutr.*, 2020, **8**, 6401–6414.

28 V. Vidya, D. Prasath, M. Snigdha, R. Gobu, C. Sona and C. S. Maiti, Development of EST-SSR markers based on transcriptome and its validation in ginger (Zingiber officinale Rosc.), *PLoS One*, 2021, **16**, e0259146.

29 X. Deng, J. Yu, M. Zhao, B. Zhao, X. Xue, C. Che, J. Meng and S. Wang, Quality assessment of crude and processed ginger by high-performance liquid chromatography with diode array detection and mass spectrometry combined with chemometrics, *J. Sep. Sci.*, 2015, **38**, 2945–2952.

30 H. B. Zhao, Z. H. Wang, F. He, H. Meng, J. H. Peng and J. L. Shi, [Analysis of Volatile Oils from Different Processed Products of Zingiber officinale Rhizome by GC-MS], *Zhongyaocai*, 2015, **38**, 723–726.

31 H. T. El-Borm, M. S. Gobara and G. M. Badawy, Ginger extract attenuates labetalol induced apoptosis, DNA damage, histological and ultrastructural changes in the heart of rat fetuses, *Saudi J. Biol. Sci.*, 2021, **28**, 440–447.

32 K. Contrepois, S. Wu, K. J. Moneghetti, D. Hornburg, S. Ahadi, M. S. Tsai, A. A. Metwally, E. Wei, B. Lee-McMullen, J. V. Quijada, S. Chen, J. W. Christle, M. Ellenberger, B. Balliu, S. Taylor, M. G. Durrant, D. A. Knowles, H. Choudhry, M. Ashland, A. Bahmani, B. Enslen, M. Amsallem, Y. Kobayashi, M. Avina, D. Perelman, S. M. Schüssler-Fiorenza Rose, W. Zhou, E. A. Ashley, S. B. Montgomery, H. Chaib, F. Haddad and M. P. Snyder, Molecular Choreography of Acute Exercise, *Cell*, 2020, **181**, 1112–1130.

33 X. Meng, X. Zhang, X. Su, X. Liu, K. Ren, C. Ning, Q. Zhang and S. Zhang, Daphnes Cortex and its licorice-processed products suppress inflammation via the TLR4/NF-κB/NLRP3 signaling pathway and regulation of the metabolic profile in the treatment of rheumatoid arthritis, *J. Ethnopharmacol.*, 2022, **283**, 114657.

34 X. Meng, J. Ma, A. N. Kang, S. Y. Kang, H. W. Jung and Y. K. Park, A Novel Approach Based on Metabolomics Coupled With Intestinal Flora Analysis and Network Pharmacology to Explain the Mechanisms of Action of Bekhogainsam Decoction in the Improvement of Symptoms of Streptozotocin-Induced Diabetic Nephropathy in Mice, *Front. Pharmacol.*, 2020, **11**, 633.

35 X. H. Miao, X. J. Feng, X. R. Yang and Y. H. Bai, Foxiangyin on the Model Rats with Cold Coagulation and Blood Stasis

Dysmenorrhea Pain Reaction and Blood Rheology, *Heb. Med.*, 2017, **23**, 1791–1795.

36 Z. G. Wu, P. Hu, B. S. Fan, S. C. Zhang, C. X. Liu and X. He, Study on the effect of Shaofu Zhuyu Decoction on promoting blood circulation in rats with primary dysmenorrhea of cold-coagulating blood stasis syndrome, *Tianjin J. Tradit. Chin. Med.*, 2020, **37**, 929–935.

37 B. Ma, S. Yang, T. Tan, J. Li, X. Zhang, H. Ouyang, M. He and Y. Feng, An integrated study of metabolomics and transcriptomics to reveal the anti-primary dysmenorrhea mechanism of Akebiae Fructus, *J. Ethnopharmacol.*, 2021, **270**, 113763.

38 X. Meng, J. Yan, J. Ma, A. N. Kang, S. Y. Kang, Q. Zhang, C. Lyu, Y. K. Park, H. W. Jung and S. Zhang, Effects of Jowiseungki-tang on high fat diet-induced obesity in mice and functional analysis on network pharmacology and metabolomics analysis, *J. Ethnopharmacol.*, 2022, **283**, 114700.

39 W. Yeo, S. L. Chan, F. K. Mo, C. M. Chu, J. W. Hui, J. H. Tong, A. W. Chan, J. Koh, E. P. Hui, H. Loong, K. Lee, L. Li, B. Ma, K. F. To and S. C. Yu, Phase I/II study of temsirolimus for patients with unresectable Hepatocellular Carcinoma (HCC)- a correlative study to explore potential biomarkers for response, *BMC Cancer*, 2015, **15**, 395.

40 H. A. Azim Jr., F. A. Peccatori, S. Brohée, D. Branstetter, S. Loi, G. Viale, M. Piccart, W. C. Dougall, G. Pruneri and C. Sotiriou, RANK-ligand (RANKL) expression in young breast cancer patients and during pregnancy, *Breast Cancer Res.*, 2015, **17**, 24.

41 A. C. Zarpelon, T. M. Cunha, J. C. Alves-Filho, L. G. Pinto, S. H. Ferreira, I. B. McInnes, D. Xu, F. Y. Liew, F. Q. Cunha and W. A. Verri Jr., IL-33/ST2 signalling contributes to carrageenin-induced innate inflammation and inflammatory pain: role of cytokines, endothelin-1 and prostaglandin E2, *Br. J. Pharmacol.*, 2013, **169**, 90–101.

42 P. W. Mantyh, Cancer pain and its impact on diagnosis, survival and quality of life, *Nat. Rev. Neurosci.*, 2006, **7**, 797–809.

43 K. Tajino, H. Hosokawa, S. Maegawa, K. Matsumura, A. Dhaka and S. Kobayashi, Cooling-sensitive TRPM8 is thermostat of skin temperature against cooling, *PLoS One*, 2011, **6**, e17504.

44 M. N. Moraes, L. V. M. de Assis, F. D. S. Henriques, M. L. Batista Jr., A. D. Güler and A. M. L. Castrucci, Cold-sensing TRPM8 channel participates in circadian control of the brown adipose tissue, *Biochim. Biophys. Acta, Mol. Cell Res.*, 2017, **1864**, 2415–2427.

45 Y. Xie, J. Qian and M. Wu, Protein expression profiling of rat uteruses with primary dysmenorrhea syndrome, *Arch. Gynecol. Obstet.*, 2022, **305**, 139–147.

46 F. Sui and T. Jiang, Study on scientific connotation of four herbal properties on basis of cold and hot perceptions, *Zhongguo Zhongyao Zazhi*, 2012, **37**, 2501–2504.

47 F. Sui, N. Lin, J. Y. Guo, C. B. Zhang, X. L. Du, B. S. Zhao, H. B. Liu, N. Yang, L. F. Li, S. Y. Guo, H. R. Huo and T. L. Jiang, Cinnamaldehyde up-regulates the mRNA expression level of TRPV1 receptor potential ion channel protein and its function in primary rat DRG neurons in vitro, *J. Asian Nat. Prod. Res.*, 2010, **12**, 76–87.

48 M. K. Choi, J. Kim, H. M. Park, C. M. Lim, T. H. Pham, H. Y. Shin, S. E. Kim, D. K. Oh and D. Y. Yoon, The DPA-derivative 11S, 17S-dihydroxy 7,9,13,15,19 (Z,E,Z,E,Z)-docosapentaenoic acid inhibits IL-6 production by inhibiting ROS production and ERK/NF-κB pathway in keratinocytes HaCaT stimulated with a fine dust PM(10), *Ecotoxicol. Environ. Saf.*, 2022, **232**, 113252.

49 M. Nakayama, M. Naito, K. Omori, S. Ono, K. Nakayama and N. Ohara, Porphyromonas gingivalis Gingipains Induce Cyclooxygenase-2 Expression and Prostaglandin E(2) Production via ERK1/2-Activated AP-1 (c-Jun/c-Fos) and IKK/NF-κB p65 Cascades, *J. Immunol.*, 2022, **208**, 1146–1154.

50 X. Meng, B. Wang, X. Zhang, C. Lyu, X. Su, C. Ning and S. Zhang, The dynamic changes and mechanisms of Rehmanniae radix processing based on Maillard reaction, *Tradit. Med. Res.*, 2021, **6**, 1–10.

51 X. Meng, Y. Liang, C. Lyu, X. Su, C. Hu, C. Ning and S. Zhang, Effects of processing technology on essential oil and pharmacological action of frankincense, *Tradit. Med. Res.*, 2021, **6**, 21–30.

52 X. Meng, X. Zhang, C. Hu, X. Su and S. Zhang, The riddles of number nine in Chinese medicine processing method, *Tradit. Med. Res.*, 2021, **6**, 11–20.

53 Y. Zhang, N. Su, W. Liu, Q. Wang, J. Sun and Y. Peng, Metabolomics Study of Guizhi Fuling Capsules in Rats With Cold Coagulation Dysmenorrhea, *Front. Pharmacol.*, 2021, **12**, 764904.

54 C. Ma, N. Liang, L. Gao and C. Jia, Danggui Sini Decoction (herbal medicine) for the treatment of primary dysmenorrhoea: a systematic review and meta-analysis, *J. Obstet. Gynaecol.*, 2021, **41**, 1001–1009.

55 Y. Xu, Q. Yang and X. Wang, Efficacy of herbal medicine (cinnamon/fennel/ginger) for primary dysmenorrhea: a systematic review and meta-analysis of randomized controlled trials, *J. Int. Med. Res.*, 2020, **48**, 300060520936179.

56 G. Y. Ma, C. J. Li, D. L. Li and H. L. Wang, Preliminary study on the external application of ginger volatile oil and gingerol for primary dysmenorrhea model of mice, *Chin. Med. Mod. Distance Educ. China*, 2020, **18**, 112–114.

57 Y. S. Kim, C. S. Hong, S. W. Lee, J. H. Nam and B. J. Kim, Effects of ginger and its pungent constituents on transient receptor potential channels, *Int. J. Mol. Med.*, 2016, **38**, 1905–1914.

58 M. Q. Yang, L. L. Ye, X. L. Liu, X. M. Qi, J. D. Lv, G. Wang, U. K. Farhan, N. Waqas, D. D. Chen, L. Han and X. H. Zhou, Gingerol activates noxious cold ion channel TRPA1 in gastrointestinal tract, *Chin. J. Nat. Med.*, 2016, **14**, 434–440.